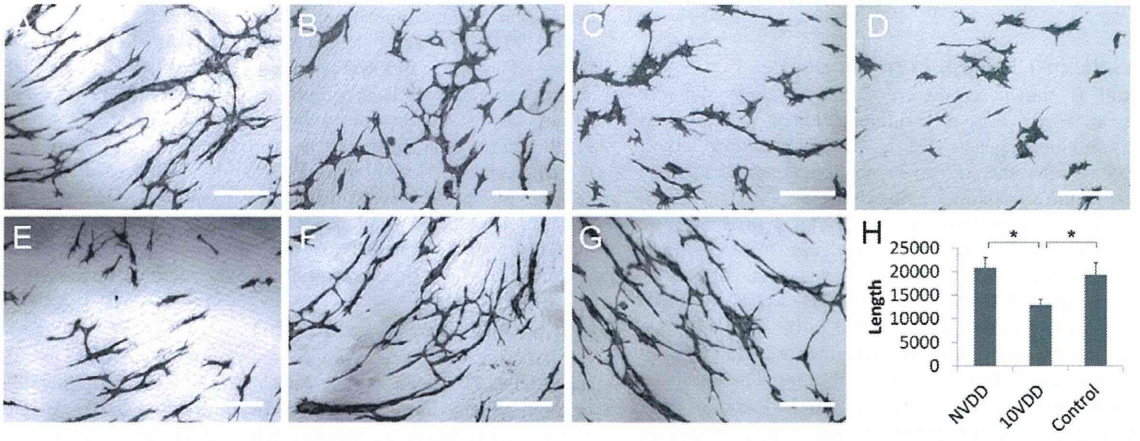

Figure 2. The activity of vasohibin-1 by an endothelial cell tube formation assay. The activity of vasohibin-1 was confirmed by an *in vitro* endothelial cell tube formation assay. Vasohibin-1 suppressed the HUVEC tube formation in a dose-dependent manner. Representative results of HUVEC tube formation treated with 2 nM VEGF combined with 0 (A), 0.2 (B), 2 (C), and 10 nM vasohibin-1 (D) are shown. Bars indicate 100 μm. The released vasohibin-1 from the device showed comparable results to native activity (E). Significant suppression of HUVEC tube formation was observed in released vasohibin-1 when compared to those treated with NVDD (F) and with only 2 nM VEGF without vasohibin-1 (G). (H) shows the average of each experiment; significantly fewer CD31-positive points were observed in released vasohibin-1-treated wells when compared to those of the vehicle released from NVDD ($p<0.0001$) or the VEGF-treated control ($p<0.0001$). The vasohibin-1 released from the device showed activity comparable to the native vasohibin-1. Vertical bar indicates total length of tube formation. NVDD: non-vasohibin-1 (vehicle) delivery device, 10VDD: 10 μM vasohibin-1 delivery device.
doi:10.1371/journal.pone.0058580.g002

observed in eyes injected with intravitreal vasohibin-1 when compared to those of the NVDD ($p = 0.000006$), VDD ($p = 0.0036$), pellet transplantation ($p = 0.000023$), and intravitreal vehicle injection groups ($p = 0.000001$) (Fig. 6B). No significant difference was observed when we compared the VDD with those

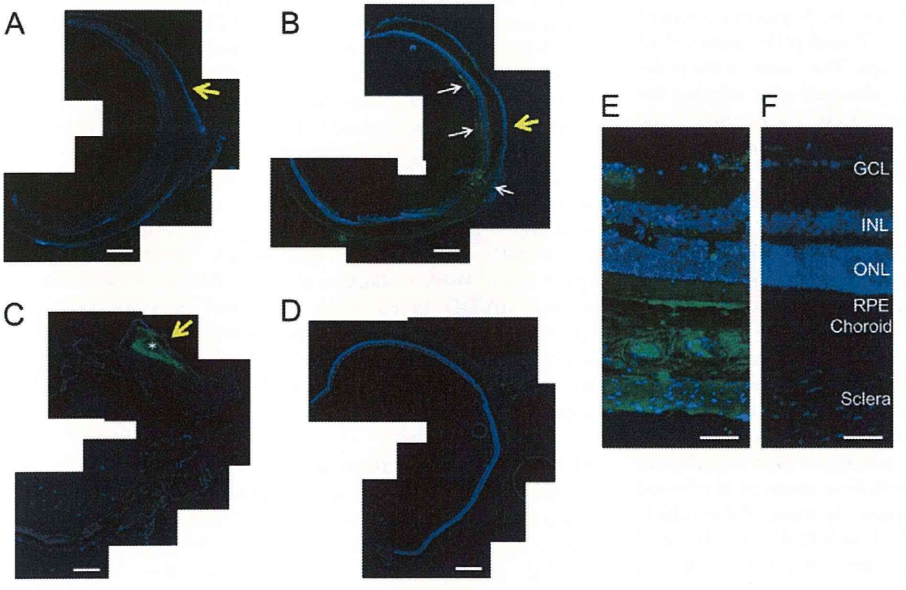

Figure 3. Immunohistochemistry of vasohibin-1 after device implantation. The immunohistochemistry results of vasohibin-1 after NVDD, 10VDD, and pellet implantation are shown. No immunoreactivity was observed after NVDD transplantation (A) and negative control without first antibody (D). 10VDD shows vasohibin-1 immunoreactivity at the device implant area (B). White arrows show the immunoreactivity in the retina and optic nerve at low magnification. Diffuse immunoreactivity was observed in the sclera, choroid, RPE, and retina at greater magnification (E). Strong immunoreactivity was observed in the ganglion cell layer (GCL) and retinal pigment epithelium (RPE), as well as in the sclera and choroid. INL and ONL indicate the inner and outer nuclear layers. These results were not observed in the NVDD group (A) or the negative controls (D and F). Strong immunoreactivity was observed in the pellet (asterisk) and in the tissues surrounding the implanted pellet (C). Yellow arrows indicate the positions where devices or pellets were placed. Devices were removed before sectioning, but pellets were not removed before sectioning. Bars: 200 μm (A–D), and 50 μm (E, F).
doi:10.1371/journal.pone.0058580.g003

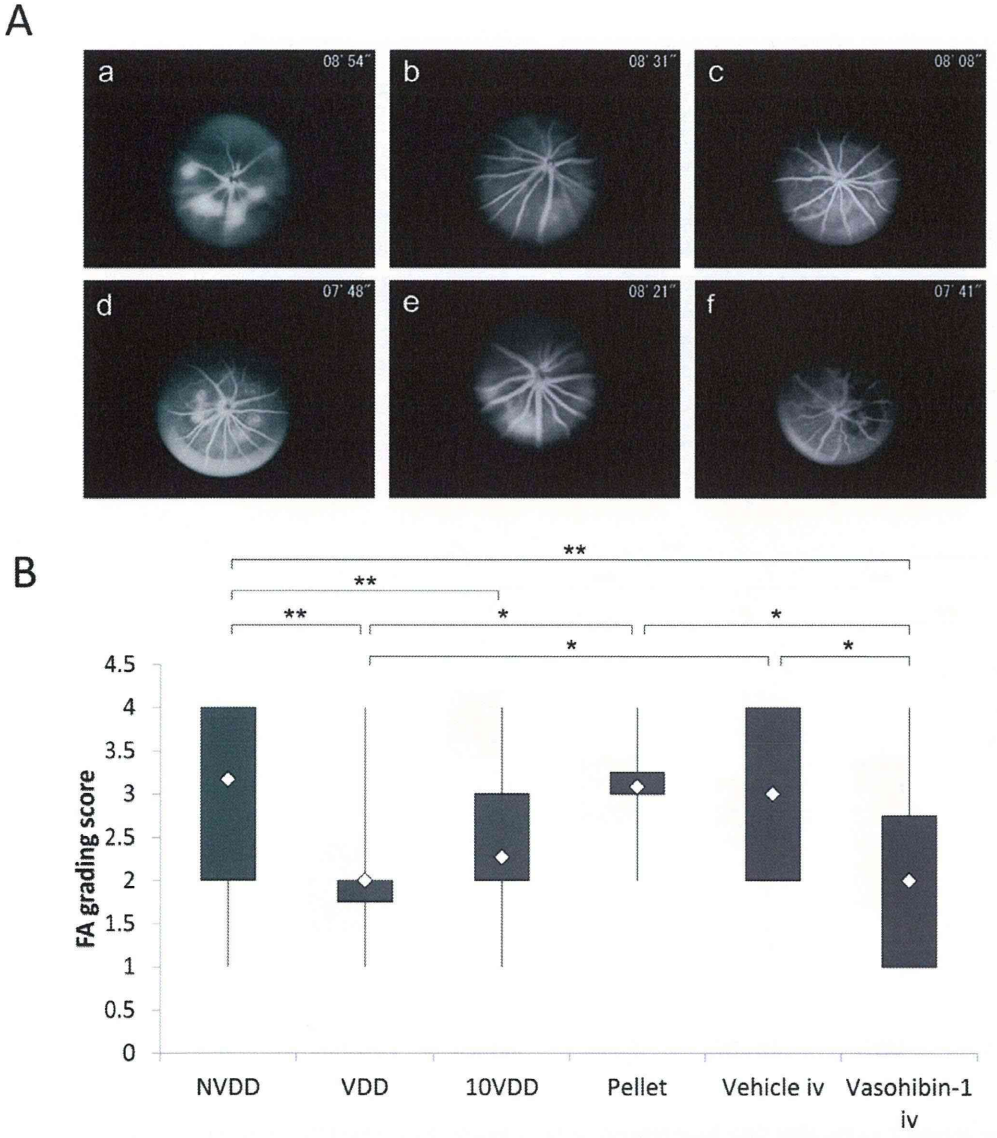

Figure 4. Fluorescein angiography 1 week after CNV laser procedure. (A) Representative results of fluorescein angiography (FA) in each group at 1 week after CNV laser procedure. The groups were treated with NVDD (a), VDD (b), 10VDD (c), vasohibin-1 pellet (d), intravitreal vehicle injection (Vehicle iv) (e), or intravitreal vasohibin-1 injection (Vasohibin-1 iv) (f). (B) Fluorescein angiography scores for each of the six laser spots in each eye are plotted and calculated for each group. Significantly lower FA scores was shown in the Vasohibin-1 iv group when compared to those of NVDD ($p = 0.00014$), pellet ($p = 0.02$), and Vehicle iv ($p = 0.040$). Significantly lower FA scores are also observed in the 10VDD group when compared to the NVDD group ($p = 0.00006$). Significantly lower FA scores are also observed in the VDD group when compared those of NVDD ($p = 0.00017$), Pellet ($p = 0.012$), and intravitreal vasohibin-1 injection ($p = 0.026$). Significant differences are shown as asterisks. NVDD: non-vasohibin-1 (vehicle) delivery device, VDD: 1 μM vasohibin-1 delivery device, 10VDD: 10 μM vasohibin-1 delivery device, Pellet: vasohibin-1 pelletized at the same concentration of 10VDD (without reservoir and cover).
doi:10.1371/journal.pone.0058580.g004

of NVDD ($p = 0.7374$), pellet transplantation ($p = 0.3616$), and intravitreal vehicle injection ($p = 0.7178$) groups.

Discussion

Attention has been paid to sustained drug delivery in the treatment of AMD because regimens including intravitreal anti-VEGF injection require repeated injection and may lead to adverse side effects [9,35]. Sustained delivery of large molecules such as antibodies may be attractive, because not only anti-VEGF therapy and anti-TNFα antibody have shown excellent results in the treatment of refractory eye diseases (such as Behcet's disease), although this regimen also requires repeated cycles of therapy [36,37]. When our devices were cultured in PBS, vasohibin-1 was released over time, with activity equivalent to that seen with native vasohibin-1. These positive results were also observed with brain-derived neurotrophic factor (BDNF) and 40 kDa dextran, as reported previously [24]. Our implantable device showed sustained protein release over time. The relatively large standard

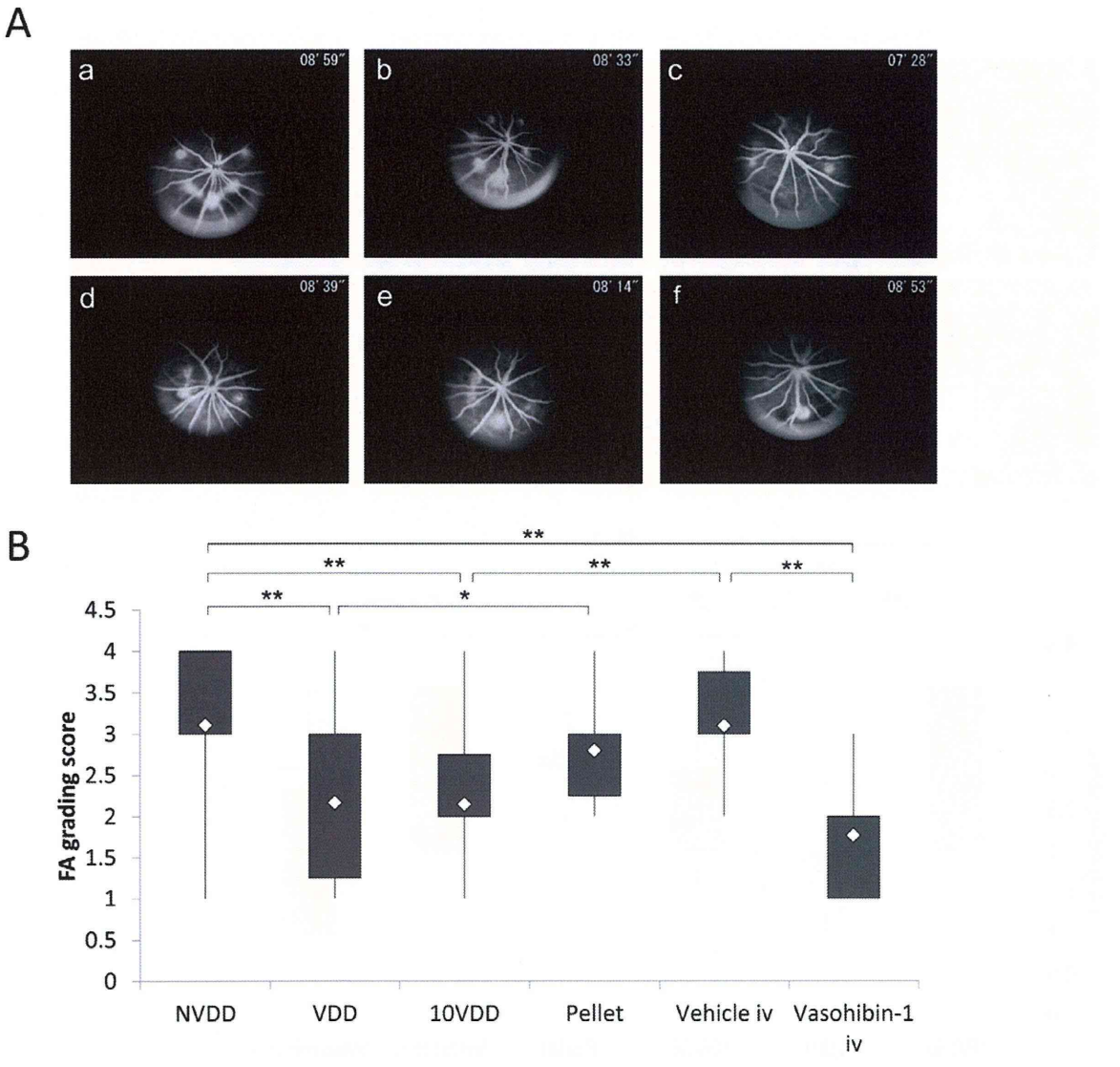

Figure 5. Fluorescein angiography 2 weeks after CNV laser procedure. (A) Representative results of fluorescein angiography in each group at 2 weeks after CNV laser procedure. The groups were treated with NVDD (a), VDD (b), 10VDD (c), vasohibin-1 pellet (d), intravitreal vehicle injection (Vehicle iv) (e), intravitreal vasohibin-1 injection (Vasohibin-1 iv) (f). (B) Significantly lower FA scores was shown in the Vasohibin-1 iv group when compared to those of NVDD ($p = 0.000022$), and Vehicle iv ($p = 0.0065$). Significantly lower FA scores are also observed in the 10VDD group when compared to the NVDD group ($p = 0.00003$) and intravitreal vehicle injection ($p = 0.011$). Significant differences are shown as asterisks. NVDD: non-vasohibin-1 (vehicle) delivery device, VDD: 1 μM vasohibin-1 delivery device, 10VDD: 10 μM vasohibin-1 delivery device, Pellets: vasohibin-1 pelletized at the same concentration of 10VDD (without reservoir and cover).
doi:10.1371/journal.pone.0058580.g005

deviation in the 10VDD group may be indicative of imperfect device preparation. From the results of western blotting, the 10VDD group showed a mild initial release of drug, although the level was far less than seen in the pellet-only group. Technical improvements in delivery device design may overcome these problems. This is an attractive device designed with sustained protein delivery for the treatment of eye diseases.

Subconjunctival drug administration produces better drug penetration than eye drops and is less invasive than intravitreal injection. However, conjunctival and episcleral blood and lymphatic flows have been reported to be the main limiting factors for posterior segment drug distribution by subconjunctival drug administration [38–40]. Our results also showed that implantation of pelletized vasohibin-1 alone (with no reservoir) produced much less vasohibin-1 immunoreactivity than seen with 10VDD implantation. Implanted between the sclera and conjunctiva, our device was designed to release the drugs only to the scleral side of the eye, so a limiting factor of drug diversion to the conjunctival blood flow may be reduced. Carvalho et al [41] reported that their tightly-sutured, one-side-open device delivered higher amount of sodium fluorescein than others, although they used small molecules with their device. From the histological analysis of our experimental procedure, we saw no signs of inflammation or adverse effects in the eye that could be attributed

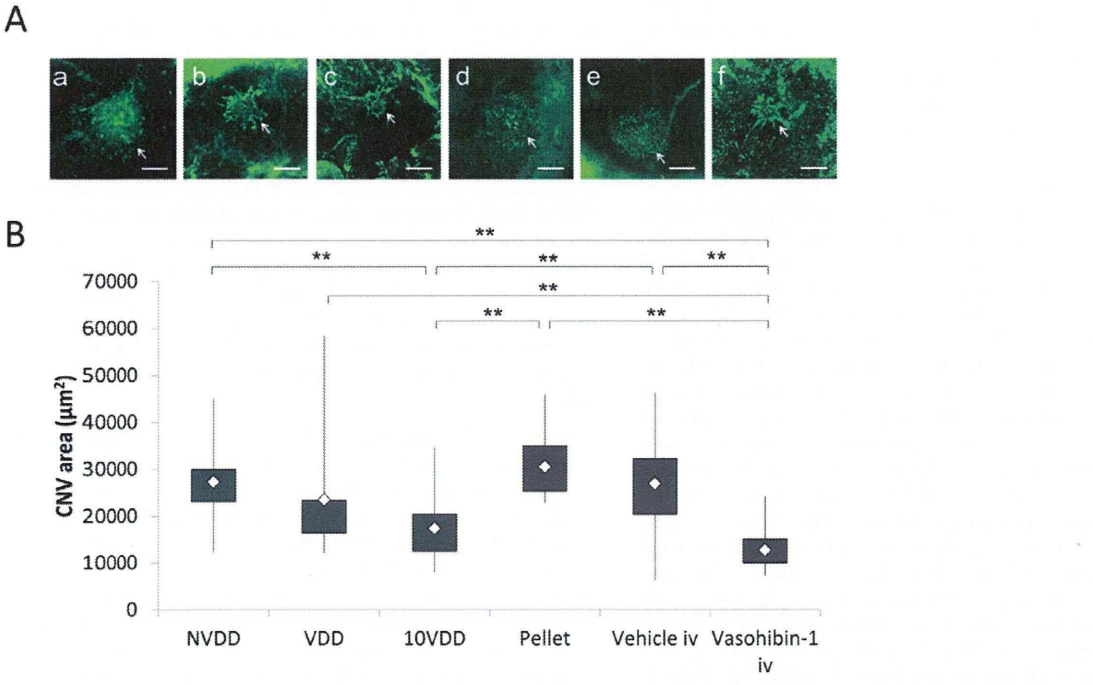

Figure 6. Flat-mount examination of the CNV site. The areas of choroidal neovascularization with devices, pellets, and intravitreal injection of recombinant vasohibin-1 protein. (A) Representative choroidal flat-mount photographs of the groups treated with NVDD (a), VDD (b), 10VDD (c), vasohibin-1 pellet (Pellet) (d), intravitreal vehicle injection (Vehicle iv) (e), intravitreal vasohibin-1 injection (Vasohibin-1 iv) (f) eyes at 2 weeks after the CNV laser procedure. Mean values of actual areas are shown in the text. Bars: 200 μm. (B) Significantly smaller CNV areas were observed in the 10VDD group when compared to those of the NVDD ($p = 0.0004$), Pellet ($p = 0.0011$), and Vehicle iv groups ($p = 0.000015$). Significantly smaller CNV areas were observed in eyes treated with Vasohibin-1 iv when compared to those treated with NVDD ($p = 0.000006$), VDD ($p = 0.0036$), Pellet ($p = 0.000023$), or Vehicle iv ($p = 0.000001$). NVDD: non-vasohibin-1 (vehicle) delivery device, VDD: 1 μM vasohibin-1 delivery device, 10VDD: 10 μM vasohibin-1 delivery device, Pellet: vasohibin-1 pelletized at the same concentration of 10VDD (without reservoir and cover).
doi:10.1371/journal.pone.0058580.g006

to device implantation, except for a mild fibrosis observed around the devices at 2 weeks post-surgery. We also found that the devices removed from the rats where fibrosis was noted showed continuing vasohibin-1 release and comparable activity when we cultured the removed device/tissues in PBS (data not shown).

Vasohibin-1 was observed on the retina at 2 weeks post-implant, principally noted in the regions where the devices were implanted. Some of the regions showed strong immunoreactivity for vasohibin-1, especially at the retinal pigmented epithelium (RPE) and the retinal ganglion cell layer (GCL); the first finding may be due to being the main outer blood-retinal barrier, while the second may be due to the vitreous-retinal barrier [42]. Vasohibin-1 released from the device may be stored in cells in these regions and later released to other regions of the retina or vitreous.

Our results demonstrated that vasohibin-1 can be delivered by our device into the retina transsclerally. Amaral et al also reported transscleral protein (pigment epithelium-derived factor and ovalbumin) delivery into the retina, although they used uncontrollable drug release via a matrix-type implant [10]. Drug released from their device was not delivered unidirectionally. Although there is a blood-retinal barrier, the penetration of such large molecules into the eye may not be so surprising. When we consider the phenomenon of some type of cancer-associated retinopathy, auto-antibodies against retinal cells or retinal-specific antigens have been reported to cause retinal dysfunction [43–45]. The elimination of proteins is reported to be one to two orders of magnitude slower than that of small molecules via the sub-conjunctival and episcleral blood flow [46], with similar results reported for the choroidal blood flow [21]. This fact may also help protein delivery to the retina with the use of our device.

Although we have not studied vasohibin-1 release from the device for more than 2 weeks *in vivo* because of the experimental design, more than 80% of the vasohibin-1 was present in the device at the end of the experimental procedure. The devices removed at the end of the experiment were still releasing vasohibin-1 (data not shown), indicating that it might be possible to use the implanted device for a longer time. These data could also indicate that we may be able to use a smaller device than those used in this experiment to deliver the same amount of drug.

Fluorescein angiography examination showed significantly lower scores in the eyes that received intravitreal vasohibin-1 than those of the intravitreal vehicle-injected eyes. The effects of vasohibin-1 were also confirmed from the flat-mount experiments. These results were same as those previously noted in mice [25]. Our 10VDD device delivered vasohibin-1 to the retina transsclerally, with results comparable to those seen with intravitreal vasohibin-1 injections. With a less invasive method than that of intravitreal injection and the added advantage of continuous drug delivery, our device may be able to replace invasive intravitreal drug injections. Although there was no significant difference between 10VDD and VDD when we evaluated by FA, a statistically significant effect was observed in only 10VDD, but not VDD when we performed the flat-mount examination. One of the reasons these two do not match exactly may be due to the uncertainty about the FA evaluation, as not only blockage by

hemorrhage, but also tissue staining and/or leakage sometimes make evaluation difficult [47]. Further study is needed to determine the exact amounts of vasohibin-1 released from the device, the kinetics of drug distribution, the correlation between drug amount and ocular distribution, and the effects of this regimen on CNV, as well as the appropriate duration of vasohibin-1 release.

Choroidal neovascularization has been reported to be produced by choriocapillaris of the choroidal blood flow [48]. Many effects of choroidal blood flow or RPE may stimulate CNV formation into the retina [49]. Drusen, a preclinical feature of age-related macular degeneration, also stimulates CNV formation [50]. Transscleral anti-CNV drug delivery will be more reasonable than that of intravitreal injection not only from the points of safety, but also from the aspect of CNV pathophysiology. The RPE and RPE-choroid complex are reported to be one to two orders of magnitude slower in drug penetration [21]. When we put our device on the sclera, the drug can pass through the sclera and reach the choroid and RPE earlier than the retina. Between the choroid and neural retina, anti-CNV drugs released from our device may suppress on-going CNV formation. Suprachoroidal bevacizumab was reported to be delivered to the RPE, choroid, and photoreceptors, whereas intravitreal injection distributed more to the inner retina [11]. Olsen et al stressed the importance of delivery of a sustained-release formulation of large molecules to the suprachoroidal space [11]. Our device will offer a safer therapeutic method than those previously reported, especially in the treatment of AMD.

Conclusion

We developed a sustained delivery device for the release of vasohibin-1 in the eye. The released vasohibin-1 showed activity comparable to vasohibin-1 delivered via other methods. When we placed the device on the rat sclera, we found vasohibin-1 released to the sclera, retinal pigment epithelium, and retina. Transscleral vasohibin-1 delivery significantly reduced laser-induced CNV that are comparable as those of effects seen with intravitreal vasohibin-1 injection in the rat eye. Our device will offer a safer therapeutic method than intravitreal injections.

Supporting Information

Figure S1 The size of the devices. The size of the device was 4 mm×4 mm×1.5 mm for the vasohibin-1 releasing assay (A, Device (a)) and 2 mm×2 mm wide ×1 mm high for the rat experiments (A, Device (b)). Because it was very difficult to detect using standard ELISA techniques, we used a larger size device for ELISA. The vasohibin-1 releasing area was 5.44 times larger in Device (a) (3.5 mm×3.5 mm = 12.25 mm^2) than that of Device (b) (1.5 mm×1.5 mm = 2.25 mm^2). Bar: 5 mm. We formulated fluorescein isothiocyanate (FITC) dextran (FD40) as simulated drugs and the device was incubated in a Transwell in 400 μL of PBS at 37°C. To estimate the amounts of FD40 that had diffused out of the Transwells, the fluorescent intensities of the PBS solutions were measured spectrofluorometrically (FluoroscanAscent; Thermo). From the results of a fitting curve (B), we calculated that the releasing rate of the larger device was 0.958 μg/hr/day, whereas the smaller device released 0.28 μg/hr/day; the difference of the releasing rates was calculated as 3.42 (0.958/0.28).
(TIF)

Figure S2 Comparison of FD40DD and FD40 pellet implantations. Rats implanted with FD40DD or FD40 pellets are shown. Devices or pellets were confirmed by color photographs (A and G), after enucleation (C and I), and after device (E) or pellet (K) removal. Mild fibrosis was observed around the devices (C) or pellets (I). FD40 was detected in the device (B), or pellets (H) by fluorescein photography at the site of the implant through the conjunctiva in the live rats during the experiment. When the eyes were enucleated at 1 week after device implantation, little fluorescence was observed in the conjunctiva and surrounding tissues (D, white arrow) in FD40DD-treated rats, whereas strong fluorescence in the conjunctiva was observed in pellet-treated rats (J, white arrow). FD40 was also detected on the sclera after removal of the device (F), but not the pellet (L) (yellow squares indicate the implantation site).
(TIF)

Acknowledgments

The authors alone are responsible for the content and writing of this paper.

Author Contributions

Conceived and designed the experiments: TA NN. Performed the experiments: HO NN HK MN YS NO TN TA. Analyzed the data: HO NN TA. Contributed reagents/materials/analysis tools: NN HK MN TA. Wrote the paper: TA.

References

1. Klein R, Peto T, Bird A, Vannewkirk MR (2004) The epidemiology of age-related macular degeneration. Am J Ophthalmol 137: 486–495.
2. (1986) Argon laser photocoagulation for neovascular maculopathy. Three-year results from randomized clinical trials. Macular Photocoagulation Study Group. Arch Ophthalmol 104: 694–701.
3. Thomas MA, Grand MG, Williams DF, Lee CM, Pesin SR, et al. (1992) Surgical management of subfoveal choroidal neovascularization. Ophthalmology 99: 952–968; discussion 975–956.
4. Eckardt C, Eckardt U, Conrad HG (1999) Macular rotation with and without counter-rotation of the globe in patients with age-related macular degeneration. Graefes Arch Clin Exp Ophthalmol 237: 313–325.
5. Reichel E, Berrocal AM, Ip M, Kroll AJ, Desai V, et al. (1999) Transpupillary thermotherapy of occult subfoveal choroidal neovascularization in patients with age-related macular degeneration. Ophthalmology 106: 1908–1914.
6. (1999) Photodynamic therapy of subfoveal choroidal neovascularization in age-related macular degeneration with verteporfin: one-year results of 2 randomized clinical trials – TAP report. Treatment of age-related macular degeneration with photodynamic therapy (TAP) Study Group. Arch Ophthalmol 117: 1329–1345.
7. Grisanti S, Tatar O (2008) The role of vascular endothelial growth factor and other endogenous interplayers in age-related macular degeneration. Prog Retin Eye Res 27: 372–390.
8. Miller JW, Adamis AP, Shima DT, D'Amore PA, Moulton RS, et al. (1994) Vascular endothelial growth factor/vascular permeability factor is temporally and spatially correlated with ocular angiogenesis in a primate model. Am J Pathol 145: 574–584.
9. Pilli S, Kotsolis A, Spaide RF, Slakter J, Freund KB, et al. (2008) Endophthalmitis associated with intravitreal anti-vascular endothelial growth factor therapy injections in an office setting. Am J Ophthalmol 145: 879–882.
10. Amaral J, Fariss RN, Campos MM, Robison WG Jr., Kim H, et al. (2005) Transscleral-RPE permeability of PEDF and ovalbumin proteins: implications for subconjunctival protein delivery. Invest Ophthalmol Vis Sci 46: 4383–4392.
11. Olsen TW, Feng X, Wabner K, Csaky K, Pambuccian S, et al. (2011) Pharmacokinetics of pars plana intravitreal injections versus microcannula suprachoroidal injections of bevacizumab in a porcine model. Invest Ophthalmol Vis Sci 52: 4749–4756.
12. Martin DF, Parks DJ, Mellow SD, Ferris FL, Walton RC, et al. (1994) Treatment of cytomegalovirus retinitis with an intraocular sustained-release ganciclovir implant. A randomized controlled clinical trial. Arch Ophthalmol 112: 1531–1539.
13. Charles NC, Freisberg L (2002) Endophthalmitis associated with extrusion of a ganciclovir implant. Am J Ophthalmol 133: 273–275.
14. Srivastava S, Taylor P, Wood LV, Lee SS, Robinson MR (2004) Post-surgical scleritis associated with the ganciclovir implant. Ophthalmic Surg Lasers Imaging 35: 254–255.

15. Cashman SM, Ramo K, Kumar-Singh R (2011) A non membrane-targeted human soluble CD59 attenuates choroidal neovascularization in a model of age related macular degeneration. PLoS One 6: e19078.
16. Campochiaro PA, Nguyen QD, Shah SM, Klein ML, Holz E, et al. (2006) Adenoviral vector-delivered pigment epithelium-derived factor for neovascular age-related macular degeneration: results of a phase I clinical trial. Hum Gene Ther 17: 167–176.
17. Chevez-Barrios P, Chintagumpala M, Mieler W, Paysse E, Boniuk M, et al. (2005) Response of retinoblastoma with vitreous tumor seeding to adenovirus-mediated delivery of thymidine kinase followed by ganciclovir. J Clin Oncol 23: 7927–7935.
18. Raghava S, Hammond M, Kompella UB (2004) Periocular routes for retinal drug delivery. Expert Opin Drug Deliv 1: 99–114.
19. Smiddy WE, Smiddy RJ, Ba'Arath B, Flynn HW Jr., Murray TG, et al. (2005) Subconjunctival antibiotics in the treatment of endophthalmitis managed without vitrectomy. Retina 25: 751–758.
20. Yasukawa T, Ogura Y, Tabata Y, Kimura H, Wiedemann P, et al. (2004) Drug delivery systems for vitreoretinal diseases. Prog Retin Eye Res 23: 253–281.
21. Ranta VP, Mannermaa E, Lummepuro K, Subrizi A, Laukkanen A, et al. (2010) Barrier analysis of periocular drug delivery to the posterior segment. J Control Release 148: 42–48.
22. Kunou N, Ogura Y, Yasukawa T, Kimura H, Miyamoto H, et al. (2000) Long-term sustained release of ganciclovir from biodegradable scleral implant for the treatment of cytomegalovirus retinitis. J Control Release 68: 263–271.
23. McHugh AJ (2005) The role of polymer membrane formation in sustained release drug delivery systems. J Control Release 109: 211–221.
24. Kawashima T, Nagai N, Kaji H, Kumasaka N, Onami H, et al. (2011) A scalable controlled-release device for transscleral drug delivery to the retina. Biomaterials 32: 1950–1956.
25. Wakusawa R, Abe T, Sato H, Sonoda H, Sato M, et al. (2011) Suppression of choroidal neovascularization by vasohibin-1, a vascular endothelium-derived angiogenic inhibitor. Invest Ophthalmol Vis Sci 52: 3272–3280.
26. Watanabe K, Hasegawa Y, Yamashita H, Shimizu K, Ding Y, et al. (2004) Vasohibin as an endothelium-derived negative feedback regulator of angiogenesis. J Clin Invest 114: 898–907.
27. Shen J, Yang X, Xiao WH, Hackett SF, Sato Y, et al. (2006) Vasohibin is up-regulated by VEGF in the retina and suppresses VEGF receptor 2 and retinal neovascularization. FASEB J 20: 723–725.
28. Onami H, Nagai N, Machida S, Kumasaka N, Wakusawa R, et al. (2012) Reduction of laser-induced choroidal neovascularization by intravitreal vasohibin-1 in monkey eyes. Retina 32: 1204–1213.
29. Heishi T, Hosaka T, Suzuki Y, Miyashita H, Oike Y, et al. (2010) Endogenous angiogenesis inhibitor vasohibin1 exhibits broad-spectrum antilymphangiogenic activity and suppresses lymph node metastasis. Am J Pathol 176: 1950–1958.
30. Ishikawa Y, Nagai N, Onami H, Kumasaka N, Wakusawa R, et al. (2012) Vasohibin-1 and retinal pigment epithelium. Adv Exp Med Biol 723: 305–310.
31. Tobe T, Ortega S, Luna JD, Ozaki H, Okamoto N, et al. (1998) Targeted disruption of the FGF2 gene does not prevent choroidal neovascularization in a murine model. Am J Pathol 153: 1641–1646.
32. Krzystolik MG, Afshari MA, Adamis AP, Gaudreault J, Gragoudas ES, et al. (2002) Prevention of experimental choroidal neovascularization with intravitreal anti-vascular endothelial growth factor antibody fragment. Arch Ophthalmol 120: 338–346.
33. Yu HG, Liu X, Kiss S, Connolly E, Gragoudas ES, et al. (2008) Increased choroidal neovascularization following laser induction in mice lacking lysyl oxidase-like 1. Invest Ophthalmol Vis Sci 49: 2599–2605.
34. Edelman JL, Castro MR (2000) Quantitative image analysis of laser-induced choroidal neovascularization in rat. Exp Eye Res 71: 523–533.
35. Regillo CD, Brown DM, Abraham P, Yue H, Ianchulev T, et al. (2008) Randomized, double-masked, sham-controlled trial of ranibizumab for neovascular age-related macular degeneration: PIER Study year 1. Am J Ophthalmol 145: 239–248.
36. Sfikakis PP, Theodossiadis PG, Katsiari CG, Kaklamanis P, Markomichelakis NN (2001) Effect of infliximab on sight-threatening panuveitis in Behcet's disease. Lancet 358: 295–296.
37. Ohno S, Nakamura S, Hori S, Shimakawa M, Kawashima H, et al. (2004) Efficacy, safety, and pharmacokinetics of multiple administration of infliximab in Behcet's disease with refractory uveoretinitis. J Rheumatol 31: 1362–1368.
38. Kim H, Csaky KG (2010) Nanoparticle-integrin antagonist C16Y peptide treatment of choroidal neovascularization in rats. J Control Release 142: 286–293.
39. Robinson MR, Lee SS, Kim H, Kim S, Lutz RJ, et al. (2006) A rabbit model for assessing the ocular barriers to the transscleral delivery of triamcinolone acetonide. Exp Eye Res 82: 479–487.
40. Lee SJ, He W, Robinson SB, Robinson MR, Csaky KG, et al. (2010) Evaluation of clearance mechanisms with transscleral drug delivery. Invest Ophthalmol Vis Sci 51: 5205–5212.
41. Pontes de Carvalho RA, Krausse ML, Murphree AL, Schmitt EE, Campochiaro PA, et al. (2006) Delivery from episcleral exoplants. Invest Ophthalmol Vis Sci 47: 4532–4539.
42. Stefansson E, Geirsdottir A, Sigurdsson H (2011) Metabolic physiology in age related macular degeneration. Prog Retin Eye Res 30: 72–80.
43. Kondo M, Sanuki R, Ueno S, Nishizawa Y, Hashimoto N, et al. (2011) Identification of autoantibodies against TRPM1 in patients with paraneoplastic retinopathy associated with ON bipolar cell dysfunction. PLoS One 6: e19911.
44. Thirkill CE, FitzGerald P, Sergott RC, Roth AM, Tyler NK, et al. (1989) Cancer-associated retinopathy (CAR syndrome) with antibodies reacting with retinal, optic-nerve, and cancer cells. N Engl J Med 321: 1589–1594.
45. Chan JW (2003) Paraneoplastic retinopathies and optic neuropathies. Surv Ophthalmol 48: 12–38.
46. Kim SH, Csaky KG, Wang NS, Lutz RJ (2008) Drug elimination kinetics following subconjunctival injection using dynamic contrast-enhanced magnetic resonance imaging. Pharm Res 25: 512–520.
47. Lassota N, Kiilgaard JF, la Cour M, Scherfig E, Prause JU (2008) Natural history of choroidal neovascularization after surgical induction in an animal model. Acta Ophthalmol 86: 495–503.
48. Hayreh SS (2010) Submacular choroidal vascular bed watershed zones and their clinical importance. Am J Ophthalmol 150: 940–941; author reply 941–942.
49. Lutty G, Grunwald J, Majji AB, Uyama M, Yoneya S (1999) Changes in choriocapillaris and retinal pigment epithelium in age-related macular degeneration. Mol Vis 5: 35.
50. Booij JC, Baas DC, Beisekeeva J, Gorgels TG, Bergen AA (2010) The dynamic nature of Bruch's membrane. Prog Retin Eye Res 29: 1–18.

Neurobiology of Disease 48 (2012) 556–567

Contents lists available at SciVerse ScienceDirect

Neurobiology of Disease

journal homepage: www.elsevier.com/locate/ynbdi

Metabolic stress response implicated in diabetic retinopathy: The role of calpain, and the therapeutic impact of calpain inhibitor

Ahmed Y. Shanab [a], Toru Nakazawa [a,*], Morin Ryu [a], Yuji Tanaka [a], Noriko Himori [a], Keiko Taguchi [b], Masayuki Yasuda [a], Ryo Watanabe [a], Jiro Takano [c], Takaomi Saido [c], Naoko Minegishi [b], Toshio Miyata [d], Toshiaki Abe [e], Masayuki Yamamoto [b]

[a] Department of Ophthalmology, Tohoku University Graduate School of Medicine, Japan
[b] Department of Medical Biochemistry, Tohoku University Graduate School of Medicine, Japan
[c] RIKEN Brain Science Institute, Laboratory for Proteolytic Neuroscience, Japan
[d] Division of Molecular Therapy, Tohoku University Graduate School of Medicine, Japan
[e] Division of Clinical Cell Therapy, Tohoku University Graduate School of Medicine, Japan

ARTICLE INFO

Article history:
Received 13 March 2012
Revised 12 July 2012
Accepted 25 July 2012
Available online 9 August 2012

Keywords:
Diabetic retinopathy
Retinal ganglion cell
Calpain
Oxidative stress
Synaptophysin
Neuroprotection

ABSTRACT

To describe how a high fat diet (HFD) and hyperglycemia initiate a sequence of calpain activation and oxidative stress associated with neuro-degenerative changes in diabetic retinopathy (DR), hyperglycemia was induced with streptozotocin in mice lacking the gene for calpastatin (CAST KO), and in mice lacking the gene for the transcription factor NF-E2 related factor 2 (Nrf2 KO). All animals were fed a HFD. Retinal ganglion cell (RGC) density was estimated by labeling with fluorogold and immunohistochemistry. A potent calpain inhibitor, SNJ-1945, was administered daily until the animals were sacrificed. In vitro, oxidative stress-induced RGC loss was evaluated in a high glucose culture medium with and without SNJ-1945. Retinal mRNA of calpain-1 and calpain-2 was measured by quantitative RT-PCR. Pre-apoptotic substrates of cleaved α-fodrin and synaptophysin protein were quantified by immunoblot analysis. Axonal damage was examined in transverse sections of the optic nerve. A HFD and hyperglycemia significantly increased RGC and axonal degeneration 3 weeks into the experiment. Levels of cleaved α-fodrin were increased. In the CAST KO mice, the neurotoxicity was augmented significantly. Gene manipulation of CAST and orally administered SNJ-1945 successfully modified calpain levels in the retina and prevented RGC death. In vitro, a high-glucose culture of retinal cells without antioxidants showed more RGC death than that with antioxidant treatment. The expression of synaptophysin was significantly suppressed by SNJ-1945 treatment. These results suggest that calpain plays a crucial role in metabolic-induced RGC degeneration caused by hyperglycemia and oxidative stress. Antioxidant and calpain inhibition offers important opportunities for future neuroprotective treatment against RGC death in various metabolic stress-induced diseases including DR.

Introduction

Diabetes mellitus (DM) affects approximately 285 million individuals worldwide (Shaw et al., 2010), and in developing countries, over 95% of all cases are type 2 diabetes (Hu, 2011). Around 21% of those patients will have some kind of retinopathy at the first time of diagnosis (Fong et al., 2004). Despite years of clinical and laboratory investigations, diabetic retinopathy (DR) remains the leading cause of blindness among diabetic patients (Resnikoff et al., 2004). Clinical diagnosis of DR still requires detection of vascular pathology, but there is clear evidence that hyperglycemia can cause abnormal neurological manifestations after only 2-weeks (Hancock and Kraft, 2004; Kizawa et al., 2006).

In the clinic, the amplitude of photopic negative response (PhNR), elicited by weak stimuli under dark-adapted conditions and driven mainly by retinal ganglion cells (RGCs) (Frishman et al., 1996), is reduced among diabetic patients, correlated with the degree of optic nerve damage (Kizawa et al., 2006). Measuring the thickness of circumpapillary retinal nerve fiber layer (cpRNFL), which serves as an index for the viability of RGC, with optical coherence topography (OCT), has also been noted to thin with the progress of DR (Costa et al., 2002). Furthermore, asymmetry of the cpRNFL has been observed by OCT in type 2 diabetes patients with no detectable ophthalmoscopical retinopathy (Chihara et al., 1993). At the cellular level, RGCs in postmortem human diabetic retinas have shown increased markers of apoptosis (Abu-El-Asrar et al., 2004). Taken together, this evidence shows that RGCs undergo apoptosis in

* Corresponding author at: Tohoku University Graduate School of Medicine, Department of Ophthalmology, 1-1 Seiryo, Aoba, Sendai, Miyagi 980-8574, Japan. Fax: +81 22 717 7298.
E-mail address: ntoru@oph.med.tohoku.ac.jp (T. Nakazawa).
Available online on ScienceDirect (www.sciencedirect.com).

0969-9961/$ – see front matter © 2012 Elsevier Inc. All rights reserved.
http://dx.doi.org/10.1016/j.nbd.2012.07.025

human eyes with diabetes, leading to a reduction in thickness of the nerve fiber layer. Consequently, it is important to clarify the pathogenesis of RGC death in DR, and develop a neuroprotective treatment to try to rescue RGCs in the early stages of the disease.

In response, we evaluated RGCs in a metabolic model of hyperglycemia, using mice fed a high fat diet (HFD) and given low doses of streptozotocin (STZ), in which low doses of STZ led to partial destruction of pancreatic beta cells and a HFD induced insulin resistance (Mu et al., 2006; Srinivasan et al., 2005). In particular, we examined the contribution of calpain and oxidative stress to hyperglycemia-induced RGC death in vivo and in vitro experiments, and investigated whether modification of the calpain state with a pharmacological inhibitor and or adding of antioxidants has the potential to be a therapeutic target for the treatment of neurodysfunction in patients with DR.

Calpains are a family of 14 calcium-regulated, intracellular cysteine proteases, which modulate cellular functions by limited, specific proteolysis (Huang and Wang, 2001). Expressed ubiquitously in the cytoplasm of mammalian cells, they play an important role in various cell processes, including cell proliferation, signal transduction and apoptosis (Perrin and Huttenlocher, 2002). Calpain-1 (μ-calpain; activated with μM Ca^{2+}) and calpain-2 (m-calpain; activated with mM Ca^{2+}) are the two major calpain isoforms (Goll et al., 2003). Calpains are activated by locally increased intracellular Ca^{2+} levels through calcium channels and intracellular stores (Camins et al., 2006), their domains will shift towards the protease core to form a compact structure (Hanna et al., 2008). It is also associated with the degradation of their substrates including α-fodrin that forms a backbone of the membrane skeleton (Nath et al., 1996), which triggers the apoptosis pathway (Stys and Jiang, 2002).

This makes inhibition of calpain signaling a therapeutic target for several pathological conditions, including DR. Levels of calpain are regulated by an endogenous specific inhibitor, calpastatin. It binds and inhibits calpain when calcium levels are high, but releases it when calcium levels fall (Hanna et al., 2007). Recently, an exogenous calpain inhibitor, SNJ-1945, which has shown a strong ability to penetrate the retinal blood barrier after oral administration (Shirasaki et al., 2005), was described to have a neuroprotective effect against retinal cell degeneration in rat and mouse glaucoma models (Oka et al., 2006; Ryu et al., 2011). In this study, we designed our experiment using mice lacking the gene for calpastatin and SNJ-1945 for investigating the role of calpain activation and possibility of neuroprotection under RGC loss induced by hyperglycemia.

On the other hand, clinical and experimental research in vivo and in vitro in recent years has documented that oxidative stress is a common cause of retinopathy (Hinokio et al., 1999; Pan et al., 2008; Sano et al., 1998). Itoh and his colleagues described how in non-oxidative stress conditions, NF-E2 related factor 2 (Nrf2), a transcriptive factor responsible for regulation of antioxidant response genes, is tethered in the cell cytoplasm by a molecule called Keap-1 and turned over rapidly by proteasomal degradation (Itoh et al., 1999). However, in response to oxidative stress, Nrf2 is stabilized, and relocates to the nucleus, finally activating antioxidant response genes. Therefore, we used mice lacking the Nrf2 gene to induce oxidative stress and evaluate the link between oxidative stress and calpain activation.

The main goal of this study was to develop a better means to identify, prevent and treat DR in its earlier stages rather than wait for the onset of vision-threatening vascular lesions.

Research design and methods

Animals

Adult (10 weeks) male C57BL/6 mice (SLC, Shizuoka, Japan), age- and sex-matched Nrf2 knockout (Nrf2 KO) mice (Itoh et al., 1997), and calpastatin knockout mice (CAST KO) (Takano et al., 2005) were used in this study. All animals were maintained and handled in accordance with the ARVO Statement for the Use of Animals in Ophthalmic and Vision Research and the guidelines from the Declaration of Helsinki and Guiding Principles in the Care and Use of Animals. All experimental procedures described in the present study were approved by the Ethics Committee for Animal Experiments at Tohoku University Graduate School of Medicine.

Mouse model of hyperglycemia

After 4 hr of fasting, hyperglycemia was induced by intraperitoneal injection of streptozotocin (STZ, 40 mg/kg body weight, Sigma, St. Louis, MO) or in the control group, citrate buffer, for five consecutive days. All the animals were fed a high fat diet (405.5 kcal energy, 24.2% protein, 13.6% fat, 3% fiber; Quick Fat, Clea, Japan, INC) at the time of STZ administration and throughout the experiment. Seven days after the first STZ treatment, SNJ-1945 (0.5 mL, 100 mg/kg) (Senju Pharmaceutical Co. Japan, Ltd.) or carboxymethylcellulose (CMC) was administered orally once a day until the animals were killed with an overdose of anesthesia. Blood was sampled from the tail vein and blood sugar was measured with a G-Checker (Gunze, Japan) before and after STZ treatment every week. Body weight was also recorded. Achievement of hyperglycemia was defined by a blood glucose level > 250 mg/dL 7-days after the last injection of STZ, and confirmed by measuring HbA_{1C} 4-weeks after the induction of hyperglycemia.

Retrograde labeling of RGCs and cell count

Retrograde labeling with fluorochrome (Fluorogold: FG, Englewood, CO) was performed as previously described by us (Nakazawa et al., 2007a). Briefly, the mice were anesthetized with a mixture of ketamine (100 mg/kg; Ketaset, Fort Dodge Animal Health, Fort Dodge, IA) and xylazine (9 mg/kg, TranquiVed; Vedco Inc., St. Joseph, MO) prepared at room temperature. Under full anesthesia, two small holes were drilled into the skull at the sites corresponding to the superior colliculi, where 2 μL of 2% FG with 1% dimethylsulfoxide (DMSO) was injected using a Hamilton syringe with a 32 G needle. Seven days after injection of FG, the mice were killed with an overdose of anesthesia; the retinas were harvested, and fixed with 4% of paraformaldehyde (PFA) overnight. The retinas were flat-mounted and the RGC density was determined by counting the FG-labeled RGCs in 12 distinct areas under the microscope (Axiovert-200; Zeiss, Germany) (Nakazawa et al., 2007a).

Quantitative RT-PCR (qRT-PCR)

qRT-PCR was performed as previously described (Nakazawa et al., 2007c) with minor modifications. Neural retinas were sampled and immediately sunk in an RNA stabilization reagent (RNase later, Sample and Assay Technology; Qiagen). Total RNA was extracted from the retinas using an extraction reagent (TRIzol; Invitrogen) and cDNA was synthesized with SuperScript III reverse transcriptase (Invitrogen). Real-time PCR was performed using a 7500 Fast Real Time PCR System (A&B Applied Biosystems, CA) with PCR primers for calpain-1 and calpain-2 designed by TaqMan Gene Expression Assays (Applied Biosystems, Foster, CA). The mRNA levels were normalized to GAPDH as an internal control.

Immunoblot assay

Immunoblotting was performed as previously described with one minor modification (Nakazawa et al., 2007b, 2008). The isolated retinas were placed in a lysis buffer (10 mmol/L Tris–HCl; pH 7.6, 100 mmol/L NaCl, 1 mmol/L EDTA, 1% Triton X-100, protease inhibitors). Each sample

was separated with SDS-PAGE and electroblotted to polyvinylidene fluoride membranes (Millipore, Bedford, MA). After blocking the membrane with 4% skim milk (Bio-Rad Laboratories), the membranes were incubated with a primary mouse monoclonal antibody against α-fodrin (1:1000, Abcam), or a polyclonal antibody against synaptophysin (1:1000, Cell Signaling) and β-tubulin (1:2000, Cell Signaling) overnight at 4 °C. The membranes were then incubated with a horseradish peroxidase-conjugated mouse immunoglobulin secondary antibody followed by avidin–biotin horseradish peroxidase complexes (Vectastain Elite ABC Kit; Vector, Burlingame, CA). The signals were visualized with chemo-luminescence (ECL Blotting Analysis System; Amersham, Arlington Heights, IL) measured by ImageJ software (Ver.1.44, Mac, US) and normalized to β-tubulin.

Immunohistochemistry

Immunohistochemistry (IHC) was performed as previously described (Nakazawa et al., 2007a, 2007b). Briefly, the retinal sections were incubated with a blocking buffer (PBS containing 10% goat serum, 0.5% gelatin, 3% bovine serum albumin, and 0.2% Tween 20) followed by a primary antibody against C38 (BM88) (Wakabayashi et al., 2010) or synaptophysin (1:200; Cell Signaling Technology, Inc.). The sections were then incubated with Alexa 488-conjugated goat anti-mouse or goat anti-rabbit IgG (1:200, Molecular Probes, Eugene) in a blocking buffer. The slides were shielded with a Vectashield mounting medium with DAPI (Vector Laboratories, Burlingame, CA). Photographs of the retina were taken using a

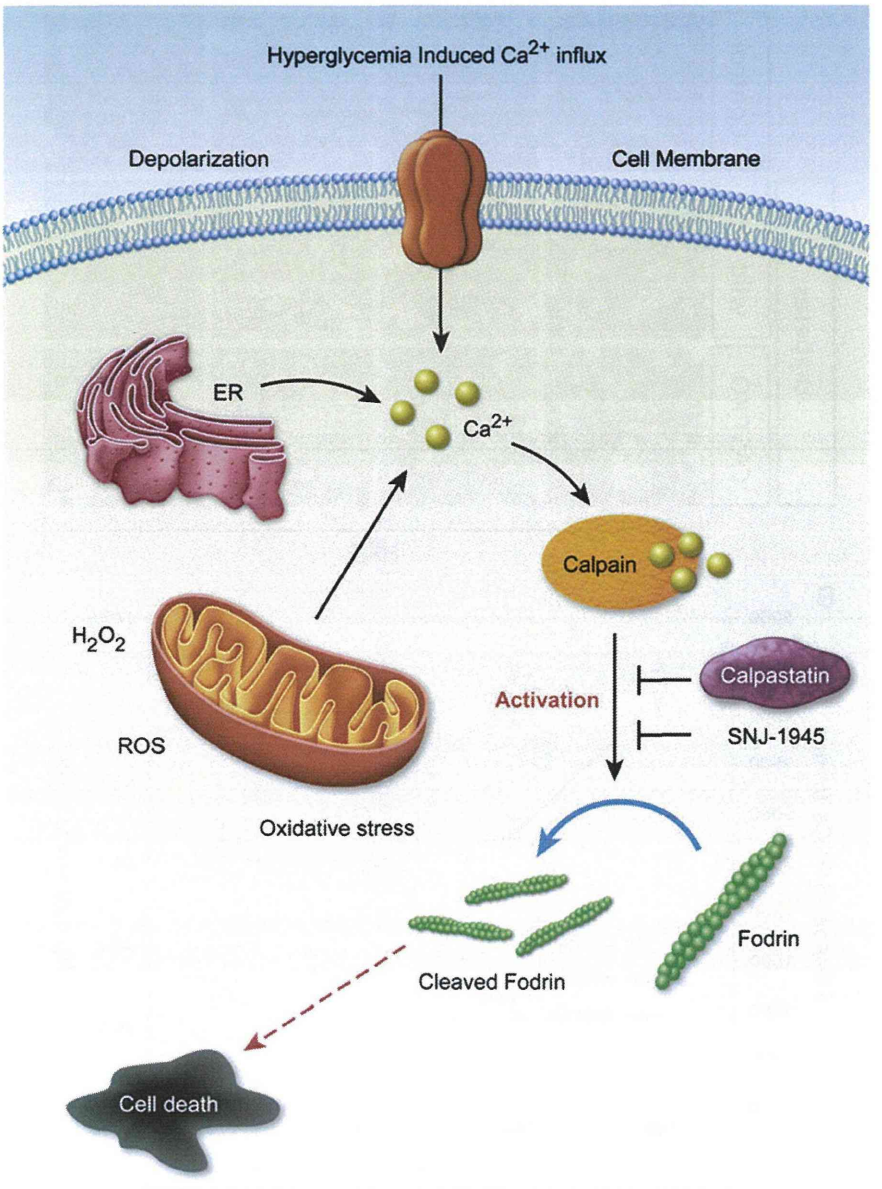

Fig. 1. Illustrative diagram showing the activation of the calpain pathway induced by Ca^{2+} ion influx overload. Hyper-excitability of the cell membrane due to hyperglycemia leads to cell membrane depolarization followed by a Ca^{2+} influx through the voltage sensitive Ca^{2+} channel. Once inside the cell, the excitation of ER and mitochondria through an increase in ROS, and the release of H_2O_2 hints at a release of more intracellular Ca^{2+}, reaching a millimolar level. Subsequently, calpain activation and cleavage leads to cell death. Calpastatin, an endogenous calpain inhibitor, showed the limitations of suppressing calpain activation. On the other hand, SNJ-1945, an exogenous calpain inhibitor, showed a more potential anti-apoptotic effect by suppressing calpain activation in the presence of a pathological intracellular Ca^{2+} level.

microscope equipped with fluorescence illumination (Axiovert-200; Zeiss, Germany).

Histological procedures for optic nerve axon analysis

To investigate the extent of hyperglycemia-induced axonal degeneration, 1 μm sections of optic nerve were processed as described in our previous publications (Nakazawa et al., 2006). Briefly, optic nerves were obtained from animals 4-weeks after STZ-induced hyperglycemia. For quantitative analyses, we analyzed five sections from each experimental condition. Optic nerves were placed immediately into a fixative consisting of 2.5% glutaraldehyde and 2% formaldehyde in 0.1 M cacodylate buffer with 0.08 M $CaCl_2$ overnight at 4 °C. The tissue was washed in 0.1 M cacodylate buffer and post-fixed in 2% aqueous OsO_4. Segments were dehydrated in graded alcohols and embedded in Epon. Then 1-μm sections were cut and stained with 1% toluidine blue in 1% borate buffer. Images were acquired using the 100× oily lens on a light microscope (BX51, Olympus) using a coupled digital camera (MP5Mc/OL, Olympus) and associated DP2-BSW software (Ver.1.3). The acquired images were quantified using Win ROOF software (Ver. 5.8.1). The number of axons was averaged per eye and expressed as numbers/mm^2.

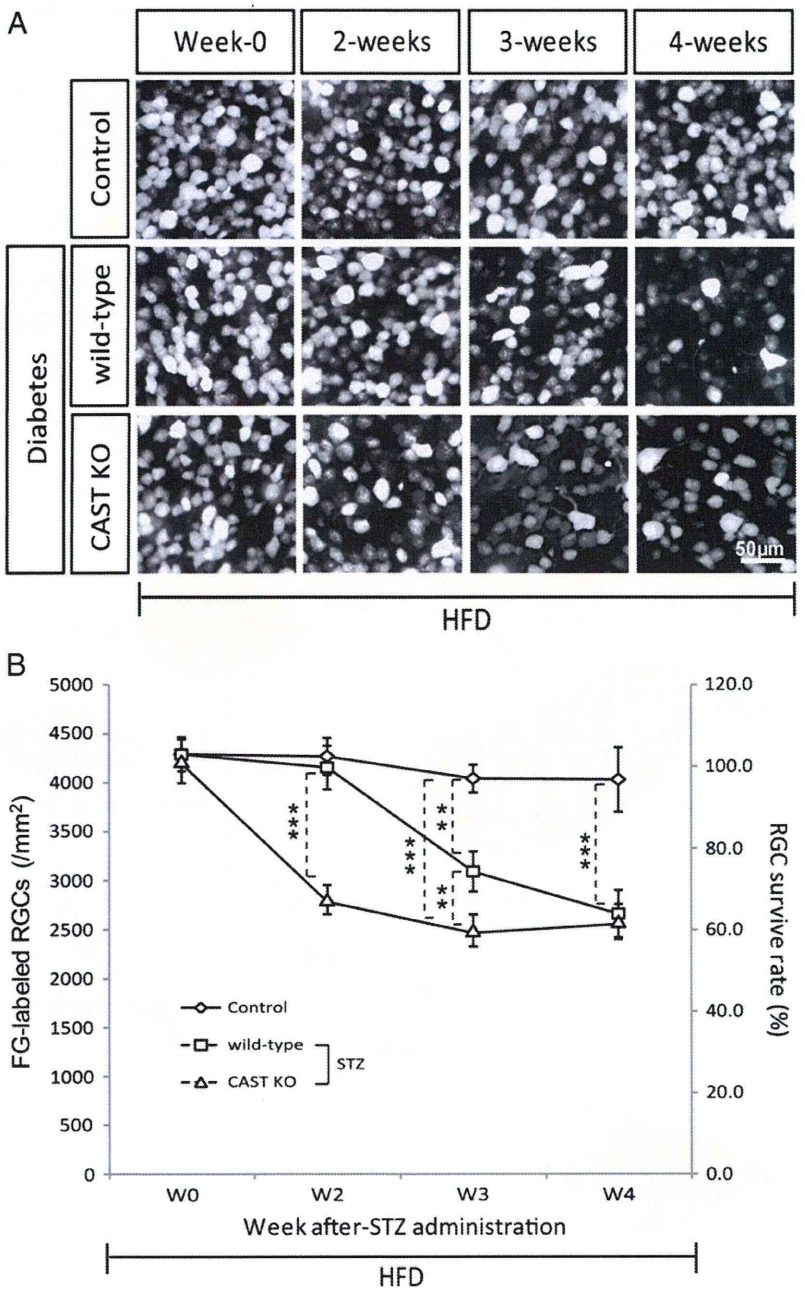

Fig. 2. Time course of fluorogold (FG)-labeled retinal ganglion cells (RGCs) with or without STZ treatment. (A) Representative photos of FG-labeled RGCs in flat-mounted retinas at four different time points (0 weeks: n = 8; two, three, and four weeks: n = 10 respectively). (B) Number of FG-labeled RGCs over time. The quantitative data of FG-labeled RGCs verified the earlier observation that the most significant degeneration was 2-weeks after STZ induction in CAST KO mice, compared to 3-weeks for wild-type mice. This showed the role of calpastatin as an endogenous calpain inhibitor and a limited delay in calpain activation in wild-type mice. Both showed around 38% RGC loss at the fourth week. **p<0.001, ***p<0.0001. Diamonds = control (citrate), squares = wild-type (STZ), triangles = CAST KO (STZ), HFD = high fat diet.